Enhancing Dye-Sensitized Solar Cell Performances by Molecular Engineering: Highly Efficient π-Extended Organic Sensitizers

Roberto Grisorio,[a] Luisa De Marco,*[b] Rita Agosta,[b] Rosabianca Iacobellis,[b, d] Roberto Giannuzzi,[b] Michele Manca,[b] Piero Mastrorilli,[a] Giuseppe Gigli,[b, c, d] and Gian Paolo Suranna*[a]

This study deals with the synthesis and characterization of two π-extended organic sensitizers (**G1** and **G2**) for applications in dye-sensitized solar cells. The materials are designed with a D–A–π–A structure constituted by i) a triarylamine group as the donor part, ii) a dithienyl-benzothiadiazole chromophore followed by iii) a further ethynylene-thiophene (**G1**) or ethynylene-benzene (**G2**) π-spacer and iv) a cyano-acrylic moiety as acceptor and anchoring part. An unusual structural extension of the π-bridge characterizes these structures. The so-configured sensitizers exhibit a broad absorption profile, the origin of which is supported by density functional theory. The absence of hypsochromic shifts as a consequence of deprotona-tion as well as notable optical and electrochemical stabilities are also observed. Concerning the performances in devices, electrochemical impedance spectroscopy indicates that the structural modification of the π-spacer mainly increases the electron lifetime of **G2** with respect to **G1**. In devices, this feature translates into a superior power conversion efficiency of **G2**, reaching 8.1 %. These results are comparable to those recorded for **N719** and are higher with respect to literature congeners, supporting further structural engineering of the π-bridge extension in the search for better performing π-extended organic sensitizers.

Introduction

Fully organic sensitizers[1] continue to capture the attention of the scientific community devoted to the development of dye-sensitized solar cells (DSSC)[2] as a competitive alternative to ruthenium(II)-based dyes.[3] Purely organic sensitizers bring advantages in terms of availability of the starting materials, design flexibility, and higher molar absorptivity with respect to

[a] Dr. R. Grisorio,+ Prof. P. Mastrorilli, Prof. G. P. Suranna
DICATECh—Dipartimento di Ingegneria Civile, Ambientale, del Territorio, Edile e di Chimica
Politecnico di Bari
Via Orabona, 4 I-70125 Bari (Italy)
E-mail: surannag@poliba.it

[b] Dr. L. De Marco,+ Dr. R. Agosta, Dr. R. Iacobellis, Dr. R. Giannuzzi, Dr. M. Manca, Prof. G. Gigli
Center for Biomolecular Nanotechnology (CBN)
Fondazione Istituto Italiano di Tecnologia (IIT)
Via Barsanti 1, 73010, Arnesano (Italy)
E-mail: luisa.demarco@iit.it

[c] Prof. G. Gigli
NNL—Istituto Nanoscienze, CNR c/o distretto tecnologico Lecce
via Arnesano 16, 73100 Lecce (Italy)

[d] Dr. R. Iacobellis, Prof. G. Gigli
Department of Mathematics and Physics "E. De Giorgi"
University of Salento, Campus Universitario
via Monteroni, 73100 Lecce (Italy)

[+] These authors contributed equally to the work.

Supporting Information for this article is available on the WWW under http://dx.doi.org/10.1002/cssc.201402164.

the inorganic dyes, providing access to several possible architectures and clearing the path towards more and more efficient DSSCs. However, compared to ruthenium dyes, most organic sensitizers generally exhibit narrower absorption bands at shorter wavelengths, resulting in less effective light-harvesting. This disadvantage is related to their commonly accepted design rule (relying on the well-known D–π–A concept) in which an electron-donating group (D) and an electron-withdrawing group (A) are connected through a suitable π-spacer (π).[4] In fact, small π-bridges are usually preferred in comparison to more π-extended spacers that do increase the portion of absorbed sunlight but, at the same time, facilitate the formation of undesired aggregates[5] and are relatively unstable when irradiated with high-energy photons.[6] However, the formation of dye aggregates can be limited by the use of suitable co-adsorbents,[7] although with unpredictable results in terms of device efficiency. Therefore, to further improve the performance of an organic dye, new design concepts should principally aim at achieving a broad spectral response, while at the same time preserving the optical and electrochemical stability of the molecule.

To this end, the incorporation of an electron-withdrawing unit into the π-bridge of a new generation of organic dyes (indicated as D–A–π–A structures) can conveniently modulate the breadth of the light-harvesting range, introducing new electronic transitions with an intramolecular charge-transfer char-

acter.[8] Furthermore, placing an acceptor moiety within the π-bridge might lead to a remarkable improvement of the dye photo-stability by increasing its oxidation potential.[9] Among the electron-withdrawing structures (such as benzotriazole,[10] quinoxaline,[11] phtalimide,[12] or diketopyrrolopyrrole[13]) successfully employed for the preparation of low band-gap organic sensitizers, benzothiadiazole can certainly be considered the most widespread unit for the obtainment of high photovoltaic performance.[14] Until now, however, little attention has been paid to the role of the π-conjugated spacer between the two acceptor units. Even a small modification of its structure could, in fact, influence both the photophysical properties of the dye and the degree of its intermolecular interactions.

Within this context, we embarked in the synthesis, characterization, and application in DSSC of the new π-extended benzothiadiazole-based structures (**G1** and **G2**, Figure 1), aiming at evaluating the impact of the π-bridge extension of the dye on the optical properties and device performances. In particular, the synthetic design envisaged the functionalization of a dithienyl-benzothiadiazole chromophore with a suitable electron-donating triarylamine group on one side and with an ethynyl-thiophene (**G1**) or with an ethynyl-benzene (**G2**) spacer, both carrying the cyano-acrylic anchoring group, on the other side. With respect to the low band-gap D–A–π–A sensitizer proposed by Grätzel and Kim (**HKK-BTZ4**, Figure 1),[14g] the introduction of the ethynylene-arylene spacer was motivated by its tendency to favor the electron-transfer process,[15] promoting the planarity of the structure and the electronic communication between the donor and the acceptor parts of the molecules. Compared to **G1**, the apparently innocent structural modification of the π-bridge (replacement of the thiophene unit with the benzene one) resulted in a remarkable improvement of the power conversion efficiencies of DSSC devices embodying **G2**, reaching a value of 8.1 % representing one of the best result thus far reported for π-extended organic sensitizers.

Results and Discussion

Synthesis

The synthetic sequence followed for the obtainment of **G1** and **G2** is illustrated in Scheme 1. A selective mono-bromination of 4,7-bis-thiophen-2-yl-benzo[2,1,3]thiadiazole was achieved with an equimolar amount of N-bromo-succinimide (NBS) to afford the corresponding bromo-derivative **1** which, in turn, was converted into the corresponding iodo-derivative **2** by reaction with N-iodo-succinimide (NIS). A Suzuki coupling between 4-(4,4,5,5-tetramethyl-1,3,2-dioxaborolan-2-yl)-N,N-bis(4-(2-ethyl-hexyloxy)phenyl)-aniline and **2** allowed the binding of the triarylamine electron-donating group to the benzothiadiazole chromophore, with the obtainment of **3**, endowed with the bromide leaving group. The introduction of the ethynylene moiety was accomplished by a Pd-catalyzed Sonogashira cross-coupling between **7** and trimethylsilyl-acetylene, to yield the alkyne **4**. The trimethylsilyl protecting group in **4** was easily removed by reaction with potassium fluoride affording the terminal alkyne **5**. At this stage, the synthetic procedure diverged for the obtainment of **G1** and **G2**. The assembly of the π-bridges was, in fact, completed by a further Sonogashira cross-coupling of **5** with either 5-bromo-thiophene-2-carbaldehyde or with 4-bromobenzaldehyde to obtain aldehydes **6** and **7**, respectively. The introduction of the cyano-acrylic functionality was carried out subjecting **6** and **7** to a Knoevenagel condensation with cyanoacetic acid in the presence of ammonium acetate eventually yielding the target molecules **G1** and **G2**, respectively. The chemical structures of the dyes as well as those of their precursors were confirmed by a combination of elemental analysis, multinuclear NMR spectroscopy, IR spectroscopy, and mass spectrometry.

Photophysical and electrochemical properties

The UV/Vis absorption spectra of **G1** and **G2** measured in THF are shown in Figure S1A, Supporting Information. The absorp-
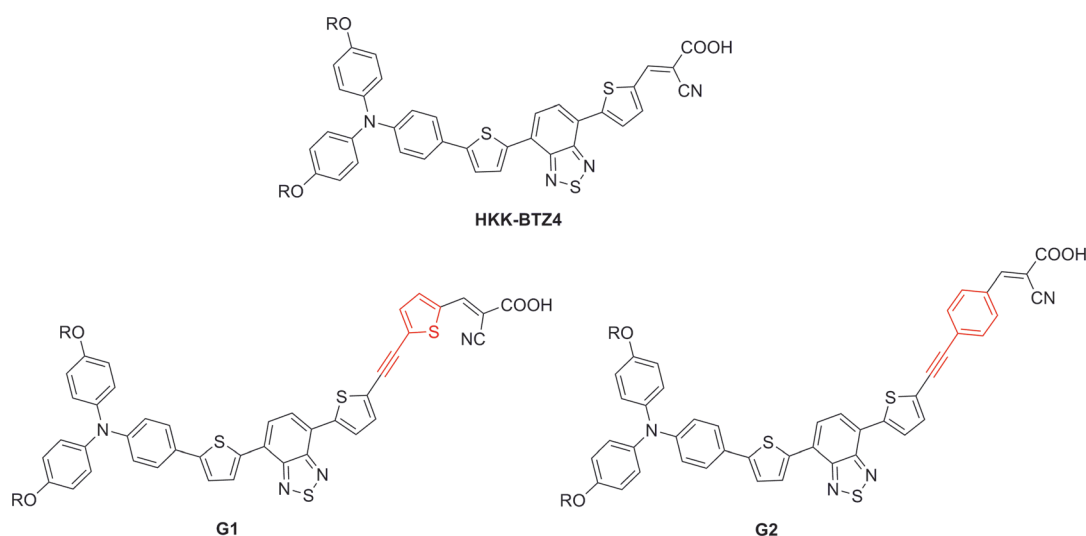
Figure 1. Chemical structure of **G1**, **G2**, and the congener **HKK-BTZ4** (R = 2-ethyl-hexyl).

These are not the final page numbers! ↗↗
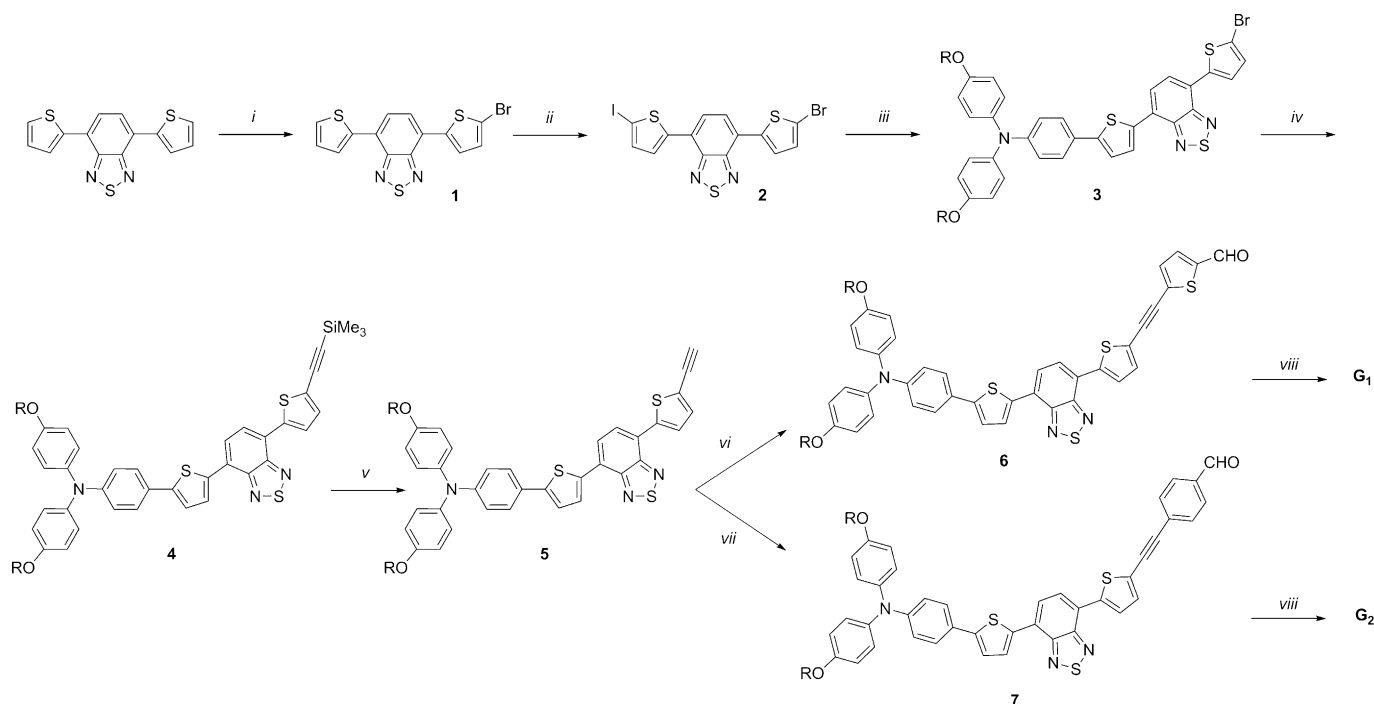
Scheme 1. Synthetic sequence for the obtainment of **G1** and **G2**. *i*: NBS, DMF, 0 °C (35 %); *ii*: NIS, CH$_2$Cl$_2$, CH$_3$COOH, rt (62 %); *iii*: 4-(4,4,5,5-tetramethyl-1,3,2-di-oxaborolan-2-yl)-*N,N*-bis(4-(2-ethyl-hexyloxy)phenyl)-aniline (1 equiv), Pd(PPh$_3$)$_4$, THF, 1 M NaHCO$_3$, reflux (74 %); *iv*: trimethylsilyl-acetylene, PdCl$_2$(PPh$_3$)$_2$, CuI, Et$_2$NH, reflux (55 %); *v*: KF, CH$_2$Cl$_2$, MeOH, 55 °C (88 %); *vi*: 5-bromo-thiophene-2-carbaldehyde, Pd(PPh$_3$)$_4$, CuI, Et$_2$NH, reflux (59 %); *vii*: 4-bromobenzaldehyde, Pd(PPh$_3$)$_4$, CuI, Et$_2$NH, reflux (53 %); *viii*: cyano-acetic acid, CH$_3$COONH$_4$, CH$_3$COOH, reflux; yield: 40 % (**G1**) and 38 % (**G2**); R = 2-ethyl-hexyl.

tion profiles of **G1** and **G2** are characterized by two main absorption bands, in analogy with other benzothiadiazole-based organic dyes.[14]

Concerning the lower energy band, the structural modification of the π-bridge did not lead to substantial differences in the absorption maxima of the two dyes, observed at 539 and 538 nm for **G1** and **G2**, respectively. Consequently, their absorption onset in THF solution was very similar (636 nm). Furthermore, the broad absorption profile in the visible region was also accompanied by high molar extinction coefficients ($\varepsilon = 24\,000$ and $20\,000$ M^{-1} cm^{-1} for **G1** and **G2**, respectively). The absorption peak in the UV region was characterized by a relatively higher intensity and appeared at 373 nm for both molecules ($\varepsilon = 28\,500$ M^{-1} cm^{-1} and $23\,200$ M^{-1} cm^{-1} for **G1** and **G2**, respectively).

Considering that the absorption spectra of organic sensitizers on mesoporous TiO$_2$ can be heavily affected by scattering effects and in order to predict the aggregation behavior of the π-extended dyes once absorbed onto the TiO$_2$ surface, the optical properties of **G1** and **G2** were investigated in the solid state as thin films on quartz substrates. Significant differences can be observed in the optical behavior of the two dyes in the solid state: in fact, inspection of Figure S1B in the Supporting Information reveals a red-shift of the absorption maximum and a remarkable broadening of the absorption profile of the thiophene-based dye **G1** ($\lambda_{max} = 551$ nm) with respect to its benzene-based counterpart **G2** ($\lambda_{max} = 541$ nm). This result indicates that the nature of the π-bridge has a remarkable influence on the solid state properties of the materials and, in par-

ticular, that the presence of the thiophene unit in **G1** seems to bring about stronger intermolecular interactions, favoring accumulated π–π interactions and leading to dye aggregation.

The solvatochromic behavior of an organic sensitizer is particularly useful in order to anticipate the modifications of the absorption profile consequent to the dye adsorption on TiO$_2$. Since in the absorption process the free −COOH group is very likely converted into a titanium carboxylate,[16] a detrimental blue-shift of the dye absorption maximum can commonly be observed, caused by the lower electron acceptor character of the carboxylate moiety with respect to the carboxylic acid group. In order to rule out aggregation and scattering effects, it was chosen to record the UV/Vis spectra of the dyes in THF solution and in the presence of an excess of a base (triethylamine, TEA) or of an acid (formic acid), as shown in Figure S2. The use of a large excess ($\approx 10^5$ mol per mol) of TEA was conceived to directly investigate in solution the optical behavior of the deprotonated form of the dye. We were pleased to find that the absorption profiles of **G1** and **G2** recorded either in the presence or in the absence of TEA were very similar and, practically superimposable in the visible region. It can be deduced that, in these D–A–π–A structures, the presence of benzothiadiazole as additional electron-withdrawing group as well as of the further π-bridge extension, reduces the contribution of the carboxylic functionality to the electronic transitions, thereby preserving the light-harvesting properties of these molecules from the blue shift induced by the deprotonation. These results were substantiated by the optical responses of **G1** and **G2** in the presence of formic acid. Again, the absence

of a significant modification in the absorption profiles rules out a dependence of the dyes absorption behavior on the protonated or deprotonated form of the carboxylic functionality.

Another photophysical issue to be investigated for a promising organic sensitizer is the dye optical stability under the operating conditions of the device. An appropriate photo-stability accelerated test was therefore carried out. The photochemical stability of **G1** and **G2** was, therefore, studied by submitting a film of the dye to a high intensity UV-irradiation in air for 20 min. The high-energy photons contained in the UV radiation constitute a significant portion ($\approx 5\%$) of the solar spectrum and can be responsible for a degradation of the dye, inducing modifications on its absorption intensity and profile.[17] Moreover, possible degradation mechanisms of the dye might involve radical pathways that can be promoted by singlet oxygen formation under UV-light irradiation.[18] The photo-oxidation treatment (Figure S3) did not promote substantial changes of either the absorbance or the absorption profile of **G1** and **G2**. Although some regions of the sensitizers, such as the electron-rich triarylamine group or the ethynylene moiety, can be considered reasonably susceptible to an easy oxidative degradation, the presence of the electron-withdrawing benzothiadiazole unit in the structure of the extended π-bridge seems to impart a remarkably high intrinsic photo-stability to the molecules.

In order to verify the feasibility of the electron injection from the excited states of an organic dye to the TiO₂ conduction band and of the possibility of dye regeneration by means of the electrolyte redox couple, the estimation of the HOMO (highest occupied molecular orbital) and LUMO energy values is mandatory. To this end, cyclic voltammetry (CV) techniques are commonly employed. A scan of the anodic region (Figure S4 and S5) revealed that **G1** and **G2** exhibit three subsequent oxidation events. However, due to the relevant contribution of the electron-donating triarylamine group to the HOMO electronic distribution (see theoretical calculations), only the first oxidation event (Figure S6 and S7) is reversible for both dyes. The evaluation of the HOMO energy levels (see the Experimental Section) led to very similar values (−5.04 and −5.03 eV) for **G1** and **G2**. The obtained results suggest that, in DSSCs, an efficient regeneration of the oxidized dyes by the iodide/triiodide couple is thermodynamically feasible, thus reducing the possibility of geminated recombination. A similar behavior is observed for the cathodic process of **G1** and **G2**, characterized by three reduction events, of which only the first is fully reversible (Figure S5 and S6). The obtained LUMO values of **G1** and **G2** are −3.16 and −3.18 eV, respectively. The calculated LUMO energy values lie above the conduction band edge of TiO₂ (−4.0 eV), ensuring sufficient driving force for electron injection from the excited dyes into the conduction band of the inorganic semiconductor. Furthermore, the obtained electrochemical band-gap of **G1** and **G2** (1.88 and 1.85 eV, respectively) is in good agreement with that obtained by optical measurements.

Together with the photo-stability, the electrochemical stability of an organic sensitizer is a critical factor in assessing the potential lifetime of a DSSC, since degradation of an organic

dye might also occur in its oxidized state. In solid state CV experiments, the molecules of the first active layer are not replaced at the electrode interface and, therefore, repeated anodic scans mimic the oxidation and regeneration cycles occurring in the device. As evident from Figure S8, the CV anodic waves of **G1** and **G2** did not undergo substantial modifications after repeated scans, revealing their electrochemical stability under oxidative conditions in the time scale of the experiment. This result hints that no decomposition occurs while **G1** and **G2** are in their oxidized states. It is reasonable to suppose that, in these sensitizers, the sufficient stabilization of the dye oxidized form, as a result of hole delocalization, inhibits degradation pathways, which, conversely, are highly favored when holes are localized on specific carbon atoms.[19] Considering that, during a single CV oxidation scan, the formed cations persist for approximately 2–3 s and that seven oxidation cycles were performed, **G1** and **G2** remained stable in their oxidized states for ≈ 15–20 s. Applying Katoh's evaluation[6a] to the electrochemical stability, a dye lifetime of 15–20 year can be conjectured for **G1** and **G2**.

Theoretical calculations

In order to provide a theoretical basis to the structure–property relationships emerging from the previously described investigations, as well as to properly discuss the behavior of the synthesized dyes in DSSC devices, we investigated appropriate models of **G1** and **G2** by density functional theory (DFT) and time-dependent DFT (TD-DFT) calculations. The calculations were carried out at the ground state on isolated molecules at the B3LYP/6-31G(d,p) level of the theory. To reduce the computational load, the 2-ethyl-hexyl chains were replaced by methyl groups. The study of the optimized geometry of the molecules was addressed first. It was found that the torsion angles between the aryl planes present on the π-bridges ranged between 0.42° and 1.91°, indicating their near-planarity, favored by the presence of the ethynylene spacers between the aryl moieties.[20]

The calculated electron density distributions of the main energetic levels along with the optimized geometry obtained for **G1** and **G2** are shown in Figure S9. Their HOMOs are very similar and mainly distributed on the electron-rich triarylamine group as well as on part of the π-bridge, suggesting that the electron binding energy for the HOMO is not sensitive to the structural difference between the two dyes, as observed for the measured redox energies. Conversely, the LUMOs of **G1** and **G2** are mainly described by the π-A segment and, therefore, localized on the anchoring group, well separated from the HOMO electronic distribution. To overcome the approximation of the Koopmans' theorem, the ionization potential (minus HOMO) of **G1** and **G2** was calculated as the difference between the total energies of the N-1-electron and N-electron states, while their electron affinities (minus LUMO) as the difference between the total energies of the N-electron and N+1-electron states.[21] All energies were calculated starting from the geometrically optimized structures of both dyes. The calculations returned the same results for the ionization potentials

These are not the final page numbers! ↗↗

of **G1** and **G2** (−5.65 eV), while a slight difference was observed for their electron affinities (−2.27 and −2.15 eV for **G1** and **G2**, respectively). Despite the discrepancy between theoretical and experimental values of ionization potential and electron affinities, attributable to the fact that calculations were carried out in vacuo, the trend observed for the calculated results strictly followed that experimentally obtained by electrochemistry. Furthermore, it is of interest to gain insights into the geometric localization of the hole of the oxidized dyes (described by the LUMO of the N-1-electron state) since an accepting molecular orbital of the oxidized sensitizer placed in proximity of the anchoring group might promote geminate recombination during operation of the DSSC, consequently lowering the overall performances.[14e] As evidenced in Figure S10, the hole of the oxidized **G2** is mainly localized on the dithienyl-benzothiadiazole segment of the π-bridge and, due to the presence of the ethynylene-phenylene spacer, distinctly separated from the anchoring portion of the sensitizer. Conversely, due to the presence of a lower energy unit (thiophene *vs* benzene), the hole of the oxidized **G1** seems to be delocalized along the entire π-bridge and extending up to the anchoring moiety. These results suggest more relevant geminate recombination effects for **G1** with respect to **G2** in DSSC devices. The stronger intermolecular interactions, indicated by the solid state optical properties of **G1** are supported by its larger calculated dipole moment (12.5 Debye) with respect to that calculated for **G2** (9.2 Debye).

A deeper understanding of the optical behavior of the two sensitizers was provided by the calculation of the vertical $S_0 \rightarrow S_n$ excitation energies at the TD-DFT level of theory using the CAM-B3LYP functional. Table 1 shows that the experimental and calculated optical data, in terms of both excitation energies and oscillator strength, are in good agreement. According to the calculation, for **G1** and **G2**, the excitation in the visible region corresponds to a $S_0 \rightarrow S_1$ transition, predominantly described as HOMO→LUMO, although with additional and significant HOMO-1→LUMO and HOMO→LUMO+1 contributions. The $S_0 \rightarrow S_2$ transition, corresponding to the absorption experimentally observed in the UV region, is mainly ascribed to a HOMO-1→LUMO transition for both **G1** and **G2**, although with other

non-negligible contributions of HOMO→LUMO+1 and HOMO-2→LUMO character. The calculated natural transition orbitals (Figure 2) show that the photo-dynamics of the two main excitations ($S_0 \rightarrow S_1$ and $S_0 \rightarrow S_2$) implies a partial shift of the electron density towards the acceptor unit of the dyes, favoring the electron transfer at the titania/dye interface.

Photovoltaic performances and electrochemical impedance analysis

Several favorable characteristics emerge, in terms of potential photovoltaic properties, from the characterization of **G1** and **G2** discussed so far, in particular, concerning their light harvesting capability as well as electrochemical and photochemical stability. Therefore, the properties of the two dyes were
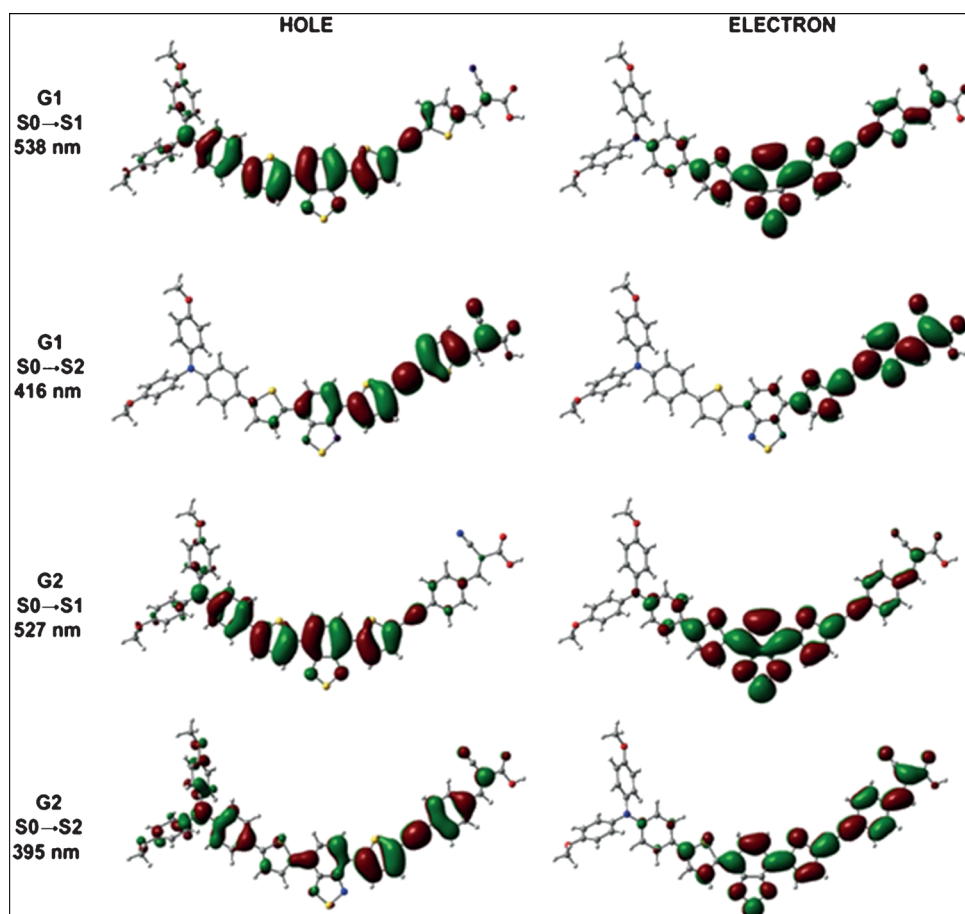
Table 1. Excitation energies, oscillator strength (*f*), and configuration of the main calculated transitions of **G1** and **G2**.

Dye	λ [nm]	*f*	Configuration
G1	538	1.93	H→L (50%); H-1→L (30%); H→L+1 (13%)
	416	0.70	H-1→L (32%); H→L+1 (30%); H-2→L (23%); H-1→L+1 (14%)
G2	527	1.66	H→L (53%); H-1→L (30%); H→L+1 (13%)
	395	0.75	H-1→L (42%); H→L+1 (29%); H-2→L (19%)

Figure 2. Calculated natural transition orbitals defining the photo-excitation dynamics in **G1** and **G2**.

These are not the final page numbers! ↗↗

tested in photo-electrochemical solar cells and their performances have also been investigated by electrochemical impedance spectroscopy (EIS).

Due to the high planarity of the sensitizers, resulting from the presence of the ethynyl-thiophene (**G1**) and of the ethynyl-benzene (**G2**) spacers, a fast intramolecular charge-transfer should be expected as well as an unfavorable π–π stacking during the uptake process, which may lead to intermolecular quenching or back transfer of the injected electrons from the TiO$_2$ conduction band. On this basis, the use of chenodeoxy-cholic acid (CDCA) as coadsorbent was evaluated. By competing with the dye for binding on the titania surface, the CDCA can, in fact, fill the gaps between the bulky sensitizers, thus minimizing detrimental dye aggregation effects.[14] Moreover, the use of a co-adsorbent such as CDCA ensures a uniform coverage of the inorganic semiconductor, thereby lowering the probability of recombination between injected electrons with I$_3^-$ and other acceptor species.[22]

Bearing this in mind, we focused on the fabrication of **G1**- and **G2**-based DSSC by the implementation of the co-adsorption strategy. We started by preparing 0.2 mm solutions of **G1** in THF with CDCA concentrations spanning the range 0–100 mm and systematically studied the influence of the amount of additive on the photovoltaic parameters, as shown in Table 2. Despite the decrease in dye loading with the increase in CDCA concentration (Table 2), the performances (Figure S11) of the **G1**-sensitized device were improved. In particular, the open-circuit voltage (V_{OC}) increased from 0.64 up to 0.69 V and the short-circuit photocurrent density (J_{SC}) raised from 7.4 up to 12.1 mA cm^{-2}, with the best results at a CDCA concentration of 80 mm. This amount of CDCA allows to achieve a power conversion efficiency (PCE) of 6.0%, while that obtained for the **G1**-sensitized devices without the addition of CDCA did not exceed 3.5% due to the effect of dye aggregation. A further increase of the CDCA concentration (100 mm) led to a decrease of both J_{SC} and V_{OC}, suggesting that, in these conditions, the additive unfavorably competes with the dye molecules for the anchoring sites.

After the screening carried out on **G1**, we decided to optimize the photovoltaic performances of **G2** (Table 2) using CDCA at 80 mm concentration. The J–V curves and the incident photon-to-current conversion efficiency (IPCE) spectra of DSSCs based on **G1** and **G2** dyes, in the presence and absence

of CDCA, are shown in Figure 3 and Figure 4, respectively. Also in the case of the **G2**-based devices, the use of CDCA significantly enhanced the performances: the J_{SC} was, in fact, increased from 10.4 mA cm^{-2} to 15.9 mA cm^{-2}. This result can be attributed to the higher electron injection efficiency in the devices obtained by **G2**/CDCA co-deposition. As expected, an in-
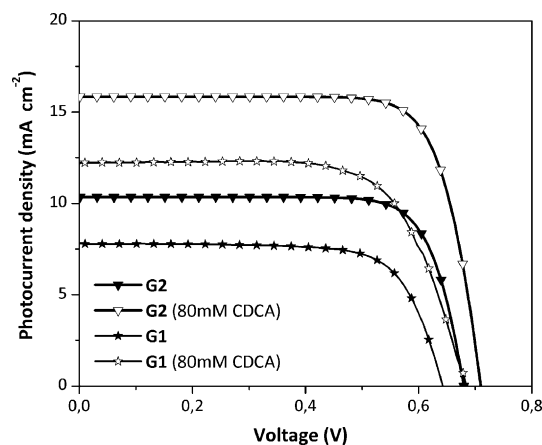

Figure 3. J–V curves of the best devices based on **G1** and **G2** dyes used as reference without or with CDCA (80 mm) under 1 sun illumination.
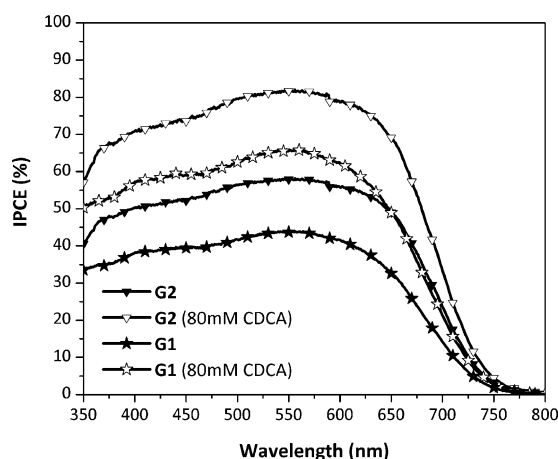

Figure 4. IPCE spectra of the best devices based on **G1** and **G2** dyes without or with CDCA (80 mm).

Table 2. Photovoltaic parameters for DSSCs based on **G1** and **G2** dyes.[a]						
Dye	CDCA [mm]	PCE [%]	V_{OC} [V]	J_{SC} [mA cm^{-2}]	FF[b]	Dye loading [mol cm^{-2}]
G1	0	3.5 (3.3 ± 0.2)	0.64 (0.65 ± 0.01)	7.4 (7.1 ± 0.3)	0.72 (0.70 ± 0.02)	3.0 × 10^{-7}
	10	4.1 (3.9 ± 0.2)	0.66 (0.67 ± 0.01)	8.4 (8.1 ± 0.5)	0.73 (0.72 ± 0.01)	2.4 × 10^{-7}
	60	5.2 (5.0 ± 0.2)	0.69 (0.69 ± 0.01)	10.4 (10.0 ± 0.4)	0.72 (0.72 ± 0.02)	1.8 × 10^{-7}
	80	6.0 (5.6 ± 0.4)	0.69 (0.69 ± 0.01)	12.2 (11.9 ± 0.4)	0.71 (0.69 ± 0.02)	1.2 × 10^{-7}
	100	4.9 (4.6 ± 0.3)	0.66 (0.65 ± 0.03)	10.3 (10.2 ± 0.3)	0.72 (0.69 ± 0.03)	0.9 × 10^{-7}
G2	0	5.1 (4.9 ± 0.2)	0.68 (0.67 ± 0.02)	10.4 (10.3 ± 0.6)	0.73 (0.71 ± 0.03)	3.4 × 10^{-7}
	80	8.1 (7.9 ± 0.2)	0.71 (0.71 ± 0.01)	15.9 (15.3 ± 0.6)	0.72 (0.72 ± 0.01)	1.3 × 10^{-7}
N719	0	8.2 (8.1 ± 0.2)	0.75 (0.75 ± 0.01)	14.8 (14.8 ± 0.7)	0.74 (0.73 ± 0.04)	2.1 × 10^{-7}
	80	2.7 (2.6 ± 0.1)	0.76 (0.77 ± 0.01)	4.2 (4.2 ± 0.3)	0.83 (0.80 ± 0.03)	0.2 × 10^{-7}
[a] Average values in parentheses are based on three replicate measurements. [b] Fill factor.						

crease in V_{OC} (from 0.68 V to 0.71 V) was also observed for the **G2**/CDCA based devices, due to the attenuation of the recombination processes with the electrolyte. As a consequence, the PCE remarkably increased from 5.1% to 8.1%, an efficiency value almost equal (99%) to that obtained for the reference devices based on commercial **N719** (8.2%), giving the highest performance in the absence of the co-adsorbent. Remarkably, the efficiency of **G1** was slightly higher than those reported for **HKK-BTZ4,** clearly pointing out the effect of the π-bridge extension.

The molecular structures of **G1** and **G2** differ only by the ethynylene-thiophene or ethynylene-benzene spacer, respectively, placed between the dithienyl-benzothiadiazole unit and the anchoring group. Nevertheless, the small structural modification on the π-bridge has a considerable effect on the DSSC performances. In fact, despite the slightly higher molar extinction coefficient of **G1**, which should lead to a better light harvesting capability, the **G2**-based devices showed slightly better performances. The superior J_{SC} value for **G2** also emerged from the IPCE spectra (Figure 4), which showed a plateau of approximately 80% at 550 nm for the **G2**/CDCA-based device compared to the plateau of approximately 60% obtained for the **G1**/CDCA-based one at 550 nm. Given that, taking the absorption and reflection of the conductive glass into account,[14f] the IPCE should not exceed the limit of ≈80–90%, it can be concluded that **G2** presents nearly unity IPCE values in the visible region.

To further investigate this aspect and the relationship between co-adsorption of CDCA and photovoltaic performance, the charge-transfer resistance and the capacitance at the TiO$_2$/dye/electrolyte interface were measured by EIS.[23] Since all devices were fabricated and tested in the same conditions, only the differences in the molecular structure of the sensitizers influenced the electrochemical parameters. EIS spectra were analyzed through the well-known equivalent circuit.[24] All electrochemical parameters have been plotted as a function of the corrected potential; the measured potential needs, in fact, to be corrected in order to take into account the losses due to the total series resistance, which lead to a potential drop that is not associated with the displacement of the Fermi level.[25]

Figure S12 and Figure S13 show the measured capacitance (C_{meas}) and the charge-transfer resistance (R_{CT}) as a function of corrected voltage for a set of devices based on **G1** and **G2** absorbed on TiO$_2$ in the absence or in the presence of CDCA (80 mM). From the analysis of C_{meas} (Figure S12), it can be noticed that the **G2**/CDCA-based devices show the most relevant downward shift of the TiO$_2$ conduction band edge. As it is well-known, the lower value of the conduction band facilitates the electron injection from the dye to the TiO$_2$ resulting in higher photocurrents. Moreover, this downward shift decreases the energy difference with the potential of the redox mediator, leading to a decrease in V_{OC}.

The lowest R_{CT} was found for the **G1**-based devices without CDCA, which confirms that injected electrons are more likely, under these conditions, to undergo recombination with the oxidized form of the redox species present in the electrolyte. The addition of CDCA to the **G1** dye solution was helpful to in-

crease the interfacial resistance of the obtained device, as indicated by the higher V_{OC} measured (Table 2), mainly due to the blocking of recombination sites. On the other hand, a counterintuitive trend of the R_{CT} was evidenced for the **G2**-based photoanodes: the **G2**/CDCA devices showed lower R_{CT} values with respect to those in which no co-adsorbent was used. This result can be interpreted by comparing the recombination resistances at a similar number of injected electrons (i.e., at the same energy difference between the electron Fermi level and the TiO$_2$ conduction band).[26] The potential scales of Figure S12 and S13 have therefore been corrected in order to take into account the shift of the conduction band due to the electron injection. In Figure S14 and S15, the reported potential scale is the equivalent conduction band voltage (V_{ecb}); the reference dye is **G2** without CDCA. Inspection of Figure S15 confirms that CDCA-based devices show the highest R_{CT} values, indicating a better suppression of charge recombination effects and explaining the higher V_{OC} observed for CDCA-based devices despite the lower value of the conduction band edge.

The electron lifetime (τ_n) in a DSSC is a fundamental parameter to assess the recombination dynamics and is defined as the average lifetime of free and trapped electrons in the TiO$_2$ before recombination with the dye oxidized form or with the oxidant in the electrolyte. It is calculated by the following equation: $\tau_n = R_{CT}C_\mu$. The trend of the apparent electron lifetime, shown in Figure 5, is in agreement with that revealed by the photovoltaic performance.

The higher electron lifetime observed for the **G1**/CDCA- and **G2**/CDCA-based DSSC confirms that the use of the coadsorbent leads to a suppression of the dark current. Comparing **G1**- and **G2**-based devices under the same test condition, **G2** shows longer electron lifetimes with respect to **G1**, implying that the recombination phenomena (geminate recombination and dark current) are considerably suppressed as also substantiated by the higher V_{OC} values. From these results, it can be deduced that the electron transfer towards the TiO$_2$ is more favored for **G2** in comparison to **G1**. As suggested by the dye loading measurements, which indicate that the amount of the dye adsorbed onto the TiO$_2$ surface for **G1** and **G2** is very simi-
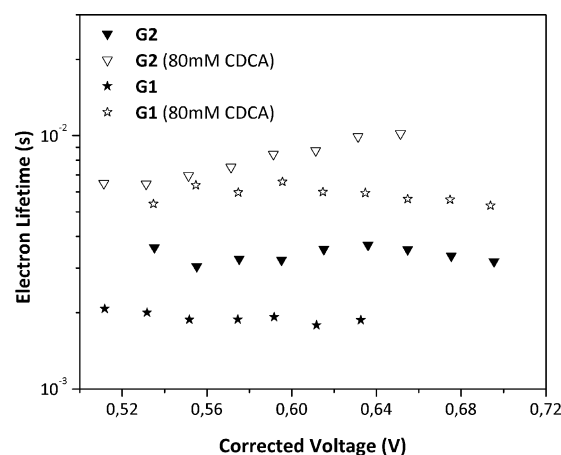

Figure 5. Apparent electron lifetime as a function of the corrected potential for DSSCs based on **G1** and **G2** dyes without or with CDCA (80 mM).

These are not the final page numbers! ↗↗

lar, it is reasonable to suppose that the CDCA presence has a lower disaggregating effect on **G1** than on **G2**. In fact, it is the higher tendency of **G1** towards aggregation due to the presence of the thiophene moiety (evidenced by the photophysical measurements) which can promote aradiative deactivation pathways for the excited states, lowering the probability of the electron injection.

On the other hand, the enhanced and unwanted electron recombination observed for the **G1**-based devices might be clarified by taking into account the potential interactions at the dye/electrolyte interface between iodine and an electron-rich heteroatom,[27] which lead to the formation of iodine-dye adducts through the following displacement reaction:

$$dye + I_3^- \rightarrow dye\text{-}I_2 + I^-.$$
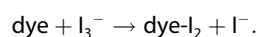
In the case of **G1**, the presence of the thiophene unit in proximity to the mesoporous semiconductor might favor the onset of a dark current by electron transfer from the titania to the coordinated iodine.

Conclusions

Aiming at evaluating the effect of the π-bridge extension on their DSSC performances, two new low band-gap sensitizers were designed with D–A–π–A structure containing: i) a triarylamine electron-donating group as the donor part, ii) a dithienylbenzothiadiazole chromophore, iii) a further ethynylene-thiophene (**G1**) or ethynylene-benzene (**G2**) π-spacer and iv) a cyano-acrylic moiety as acceptor and anchoring part. Regarding the classical weak points of the organic sensitizers (i.e., light-harvesting, stability), the new configuration brings several advantages: i) a broad absorption profile spanning the range 350–700 nm; ii) the absence of hypsochromic shifts (the origin of which was substantiated by density functional theory) as a consequence of deprotonation, ascribable to the uncommon length of the π-bridge and the simultaneous presence of the electron-withdrawing benzothiadiazole unit; iii) an appreciable optical stability, ascertained by accelerated photo-degradation test, indicating the preservation of the light-harvesting properties of the synthesized organic dyes in DSSC devices; iv) a considerable electrochemical stability as thin films in the voltammetric oxidation/re-reduction cycles that suggest a remarkable dye stability also in their oxidized form. The interpretation on the optical and electrochemical properties of **G1** and **G2** were supported by DFT calculations. Indeed, the π-bridge structural modification on **G1** and **G2** seems to have a significant influence on dye aggregation and charge recombination, as pointed out by electrochemical impedance spectroscopy. In DSSC devices, the higher electron injection efficiency and injected electron lifetimes observed for **G2** led to a superior power conversion efficiency, reaching 8.1% obtained with a suitable amount of a co-adsorbent (CDCA). Its performances are remarkably higher than those exhibited by **G1** (6.0%) and slightly higher than those of literature congeners. Despite the serious problems of dye aggregation, overcome by the use of high amounts of CDCA (80 mM), these results indicate that π-

bridge extension is a viable strategy to improve dye efficiency and suggest analogous structural engineering of known low band-gap dyes as a promising strategy to obtain even more efficient organic sensitizers.

Experimental Section

General remarks: All reactants were purchased from standard commercial sources and used without any further purification. All solvents used were carefully dried and freshly distilled according to standard laboratory practice. All manipulations were carried out under inert nitrogen atmosphere. The synthesis of 4-(4,4,5,5-tetramethyl-1,3,2-dioxaborolan-2-yl)-*N,N*-bis(4-(2-ethyl-hexyloxy)phenyl)-aniline and 4,7-bis-thiophen-2-yl-benzo[2,1,3]thiadiazole were carried out according to a literature procedure.[14g] Flash chromatography was performed using a silica gel of 230–400 mesh. ^{1}H and ^{13}C{^{1}H} NMR spectra were recorded on a Bruker Avance 700 MHz instrument. Melting points were measured on a Büchi B-545 instrument. Elemental analyses were obtained on a EuroVector CHNS EA3000 elemental analyser on the basis of three replicates. FTIR measurements were carried out on a JASCO FTIR 4200 spectrophotometer. UV/Vis spectra were recorded on a Jasco V-670 instrument. UV-photodecomposition experiments were carried out by irradiating the sample with a 150 W high-pressure Hg lamp for 20 min. High resolution electrospray ionization mass spectrometry (HR ESI-MS) analyses were performed using a Bruker microTOF QII instrument equipped with an electrospray ion source. The sample solutions (CH_2Cl_2/MeOH) were introduced by continuous infusion at a flow rate of 180 μL min^{-1} with the aid of a syringe pump. The instrument was operated in positive (negative) ion mode with endplate offset and capillary voltages set to -500 V (500 V) and -4500 V (3500 V), respectively. The nebulizer (N_2) pressure was 0.8 bar, and the drying gas (N_2) flow rate was 7.0 L min^{-1}. The capillary exit and skimmer voltages were 90 V and 30 V, respectively. The drying gas temperature was 180 °C. The calibration was carried out with sodium formate. Cyclic voltammetry was carried out on a Metrohm Autolab PGSTAT 302-N potentiostat. The materials were drop cast on a platinum working electrode from a 1 mg mL^{-1} THF solution. Measurements were carried at 25 °C in acetonitrile solution containing tetrabutylammonium tetrafluoroborate (0.025 M) as supporting electrolyte with a scan rate of 50 mV s^{-1}. The potentials were measured versus Ag/Ag$^+$ as the quasi-reference electrode. After each experiment, the potential of the Ag/Ag$^+$ electrode was calibrated against the ferrocene/ferrocenium (Fc/Fc$^+$) redox couple. The electrochemical energy gap was determined as the difference between the onsets of the oxidation and the reduction potentials ($E_g^{elc} = E_{ox}^{onset} - E_{red}^{onset}$). The HOMO and LUMO energy values were estimated from the onset potentials of the first oxidation and reduction event, respectively. After calibration against Fc/Fc$^+$, the HOMO and LUMO energy levels were calculated according to the following equations:[28]

$$E_{HOMO} \ (eV) = -[E_{ox}^{onset} - E_{1/2}(Fc/Fc^+) + 4.8]$$

$$E_{LUMO} \ (eV) = -[E_{red}^{onset} - E_{1/2}(Fc/Fc^+) + 4.8]$$

where $E_{1/2}(Fc/Fc^+)$ is the half-wave potential of the Fc/Fc$^+$ couple (the formal potential of which is assumed to be 4.8 eV in the Fermi scale) against the Ag/Ag$^+$ electrode. Analyses of the ground-state structures for the molecules were carried out by density functional theory (DFT) calculations. The B3LYP function was used in conjunction with the 6-31G(d,p) basis set. Time-dependent DFT (TD-DFT) was applied for the assessment of the excited-state transition ener-

gies. All calculations were carried out with the Gaussian 09 program package[29] and performed on isolated molecules in vacuo.

Fabrication of DSSC and photovoltaic measurement: Fluorine-doped tin oxide (FTO, 15 Ω sq^{-1}, provided by Solaronix S.A.) glass plates were first cleaned in a detergent solution using an ultrasonic bath for 15 min, and then rinsed with water and ethanol. Double-layer electrodes (overall thickness 19 μm) were prepared as follows: a layer of commercial colloidal titania paste (Dyesol 18NR-T) was deposited onto the FTO glass and gradually heated in an oven in air to obtain a ~14 μm transparent nanocrystalline film; the temperature gradient was programmed as follows: 170 °C (40 min), 350 °C (15 min), and 430 °C (30 min). This procedure was repeated for the scattering layer (5 μm) constituted by Solaronix D/SP colloidal paste. The double-layer electrode was eventually sintered at 450 °C for 30 min. The thickness and the active area (0.16 cm^2) of the sintered photoanodes was measured using a profilometer (Veeco Dektak 150 Surface Profiler). The dye loading was performed by keeping the electrodes for 14 h and under dark in 0.2 mM THF solutions of **G1** and **G2** containing, where needed, a known amount of chenodeoxycholic acid (CDCA). The reference photoanodes were prepared analogously by dyeing the electrodes with 0.2 mM solutions of bis(tetrabutylammonium)-cis-di(thiocyanato)-N,N'-bis(4-carboxylato-4'-carboxylic acid-2,2'-bipyridine) ruthenium(II) (**N719**, purchased by Solaronix S.A.) in a mixture of acetonitrile and tert-butyl alcohol (1:1 v/v). In order to evaluate the dye loading capability, the sensitized photoelectrodes were placed in a solution of tetrabutylammonium hydroxide in DMF (0.05 M) for 14 h, whereas the **N719**-sensitized photoelectrodes were immersed in a NaOH aqueous solution (0.01 M). The complete desorption was testified by the substrate discoloration. The evaluation of the dye concentration in the solvent, obtained by UV/Vis measurements, allowed the calculation of the amount of the adsorbed sensitizer, expressed in terms of moles of dye anchored per projected unit area of the photoelectrode. The counter-electrodes were prepared by sputtering a 50 nm Pt layer on a hole-drilled cleaned FTO plate. In a typical device construction procedure, the photoanode and the counter-electrode were faced and assembled using a suitably cut 50 μm thick Surlyn hot-melt gasket for sealing. The redox electrolyte (0.1 M LiI, 0.02 M I$_2$, 0.6 M 1-methyl-3-propylimidazolium iodide, and 0.5 M tert-butylpyridine in dry acetonitrile) was vacuum-injected into the space between the electrodes through pre-drilled holes on the back of the counter electrode. The holes were eventually sealed using Surlyn hot melt film and a cover glass. Photocurrent–voltage measurements were performed using a Keithley unit (Model 2400 Source Meter). A Newport AM 1.5 Solar Simulator (Model 91160A equipped with a 1000 W xenon arc lamp) serving as a light source. The light intensity (or radiant power) was calibrated to 100 mW cm^{-2} using as reference a Si solar cell. A mask with an aperture area of 0.25 cm^2 was applied to the devices before measurements. The IPCE was measured by the DC method using a computer-controlled xenon arc lamp (Newport, 140 W, 67005) coupled with a monochromator (Newport Cornerstore 260 Oriel 74125). The light intensity was measured by a calibrated silicon UV-photodetector (Oriel 71675) and the short circuit currents of the DSSCs were measured by using a dual channel optical power/energy meter, (Newport 2936-C). EIS was performed by an AUTOLAB PGSTAT 302N (Eco Chemie B.V.) in a frequency range between 100 kHz and 10 mHz. The impedance measurements were carried out at different voltage biases under 1.0 sun illumination. The resulting impedance spectra were fitted by using ZView (Scribner Associates) software.

Synthesis of 4-(5-bromo-thiophen-2-yl)-7-(thiophen-2-yl)-benzo-[2,1,3]thiadiazole (1): A solution of N-bromo-succinimide (0.89 g, 5.00 mmol) in DMF (30 mL) was added dropwise to a solution of 4,7-bis-thiophen-2-yl-benzo[2,1,3]thiadiazole (1.51 g, 5.00 mmol) in DMF (45 mL) kept at 0 °C. After the addition, the obtained reaction mixture was warmed to room temperature and allowed to react for further 2 h before quenching with water (50 mL). The compound was extracted with diethyl ether (3×50 mL) and the combined organic phases were washed with brine and dried over Na$_2$SO$_4$. After solvent removal, the crude product was purified by column chromatography (SiO$_2$, petroleum ether 40–60 °C/CH$_2$Cl$_2$ = 4:1 v/v) followed by crystallization with ethanol to afford **1** (0.65 g, 35%) as a red solid (mp: 117.5±0.5 °C). ^{1}H NMR (700 MHz, CDCl$_3$): δ = 8.11 (dd, J = 3.7, 1.1 Hz, 1 H), 7.86–7.73 (m, 3 H), 7.46 (dd, J = 5.0, 1.0 Hz, 1 H), 7.20 (dd, J = 5.0, 3.9 Hz, 1 H), 7.14 ppm (d, J = 3.9 Hz, 1 H). ^{13}C{^{1}H} NMR (176 MHz, CDCl$_3$): δ = 152.6, 152.2, 140.8, 139.3, 130.8, 128.1, 127.6, 127.4, 126.9, 126.4, 125.8, 125.1, 125.0, 114.6 ppm. HRMS (ESI) m/z: [M+Na]$^+$ calcd for C$_{14}$H$_7$BrN$_2$S$_3$Na: 402.8825; found: 402.8873. IR (KBr): $\tilde{\nu}_{max}$ = 3090, 1481, 1423, 1215, 879, 833 cm^{-1}. Elemental analysis calcd for C$_{14}$H$_7$BrN$_2$S$_3$: C 44.33, H 1.86, N 7.39; found: C 44.17, H 1.86, N 7.36.

Synthesis of 4-(5-iodo-thiophen-2-yl)-7-(5-bromo-thiophen-2-yl)-benzo[2,1,3]thiadiazole (2): N-iodo-succinimide (NIS, 0.56 g, 2.47 mmol) was added portionwise to a solution of **1** (0.75 g, 1.98 mmol) in CH$_2$Cl$_2$ (50 mL) and CH$_3$COOH (50 mL) at room temperature. The resulting mixture was allowed to react overnight before the addition of water (50 mL). The organic phase was then separated and dried over Na$_2$SO$_4$. Product **2** (0.62 g, 62%) was obtained by solvent removal as a dark red solid; mp: 215.3±0.5 °C. ^{1}H NMR (700 MHz, CDCl$_3$): δ = 7.84–7.81 (m, 3 H), 7.74 (d, J = 4.0 Hz, 1 H), 7.37 (d, J = 4.0, 1 H), 7.18 ppm (d, J = 4.0 Hz, 1 H). ^{13}C{^{1}H} NMR (176 MHz, CDCl$_3$): δ = 152.3, 152.2, 145.1, 140.6, 137.8, 130.8, 128.49, 128.47, 127.4, 125.5, 125.31, 125.27, 125.1, 114.8 ppm. HRMS (ESI) m/z: [M+Na]$^+$ calcd for C$_{14}$H$_6$BrIN$_2$S$_3$Na, 528.7791; found: 528.7002. IR (KBr): $\tilde{\nu}_{max}$ = 3081, 1480, 1412, 1214, 1074, 872, 832, 792, 509 cm^{-1}. Elemental analysis calcd for C$_{14}$H$_6$BrIN$_2$S$_3$: C 33.28, H 1.20, N 5.54; found: C 33.34, H 1.20, N 5.52.

Synthesis of 4-(5-((7-(5-bromo-thiophen-2-yl)-benzo-[2,1,3]thiadiazol-4-yl)-thiophen-2-yl)-N,N-bis(4-(2-ethyl-hexyloxy)phenyl)-aniline (3): A mixture of 4-(4,4,5,5-tetramethyl-1,3,2-dioxaborolan-2-yl)-N,N-bis(4-(2-ethyl-hexyloxy)phenyl)-aniline (1.18 g, 1.88 mmol), **2** (0.95 g, 1.88 mmol) and Pd(PPh$_3$)$_4$ (0.11 g, 9.4×10^{-2} mmol) in THF (24 mL) and a 1 M NaHCO$_3$ aqueous solution (18 mL) was refluxed for 24 h. After cooling down the reaction to room temperature, methylene chloride (50 mL) was added to the mixture and the resulting organic phase was separated, washed with water (50 mL) and dried over Na$_2$SO$_4$. After solvent removal, the crude product was purified by column chromatography (SiO$_2$, petroleum ether (40–60 °C)/CH$_2$Cl$_2$ = 7:3 v/v) to obtain **3** (1.23 g, 74%) as a purple solid, mp: 63.6±0.5 °C. ^{1}H NMR (700 MHz, CDCl$_3$): δ = 8.12 (d, J = 3.9 Hz, 1 H), 7.86–7.77 (m, 4 H), 7.51 (d, J = 8.7 Hz, 2 H), 7.16 (d, J = 4.0 Hz, 1 H), 7.10 (d, J = 8.7 Hz, 4 H), 6.96 (d, J = 8.5 Hz, 2 H), 6.87 (d, J = 8.7 Hz, 4 H), 3.91–3.81 (m, 4 H), 1.79–1.71 (m, 2 H), 1.57–1.39 (m, 8 H), 1.38–1.32 (m, 8 H), 1.00–0.91 ppm (m, 12 H). ^{13}C{^{1}H} NMR (176 MHz, CDCl$_3$): δ = 156.1, 152.44, 152.40, 146.4, 140.9, 140.2, 137.8, 137.0, 130.74, 130.66, 129.1, 127.4, 126.9, 126.8, 126.5, 125.3, 124.8, 124.4, 122.7, 120.1, 115.4, 114.3, 70.8, 39.5, 30.6, 29.1, 23.9, 23.1, 14.1, 11.2 ppm. HRMS (ESI) m/z: [M]$^+$ calcd for C$_{48}$H$_{52}$BrN$_3$O$_2$S$_3$, 879.2387; found: 879.2433. IR (KBr): $\tilde{\nu}_{max}$ = 3038, 2950, 1600, 1318, 1106, 1033, 827, 722, 511 cm^{-1}. Elemental analysis calcd for C$_{48}$H$_{52}$BrN$_3$O$_2$S$_3$: C 65.58, H 5.96, N 4.78; found: C 65.51, H 5.98, N 4.76.

Synthesis of 4-(5-((7-(5-trimethylsilylethynyl-thiophen-2-yl)-benzo[2,1,3]thiadiazol-4-yl)-thiophen-2-yl)-N,N-bis(4-(2-ethyl-hexyloxy)phenyl)-aniline (4): A mixture of **3** (0.70 g, 0.80 mmol), PdCl$_2$(PPh$_3$)$_2$ (28.1 mg, 4.0×10^{-2} mmol), CuI (3.8 mg, 2.0×10^{-2} mmol), trimethylsilyl-acetylene (0.10 g, 1.03 mmol) in diethyla-

These are not the final page numbers! ⤢⤢

mine (10 mL) was refluxed overnight. After cooling down the reaction to room temperature, methylene chloride (50 mL) was added to the mixture and the resulting organic phase was washed with water (50 mL) and dried over Na_2SO_4. After solvent removal, the crude product was purified by column chromatography (SiO_2, petroleum ether (40–60 °C)/CH_2Cl_2 = 7/3 v/v) to obtain **4** (0.39 g, 55%) as a purple solid; mp: 69.3 ± 0.5 °C. ^{1}H NMR (700 MHz, $CDCl_3$): δ = 8.14 (d, J = 3.9 Hz, 1 H), 7.96 (d, J = 3.9 Hz, 1 H), 7.88–7.85 (m, 2 H), 7.51 (d, J = 8.7 Hz, 2 H), 7.34–7.29 (m, 2 H), 7.10 (d, J = 8.7 Hz, 4 H), 6.96 (d, J = 8.5 Hz, 2 H), 6.87 (d, J = 8.7 Hz, 4 H), 3.89–3.82 (m, 4 H), 1.76–1.72 (m, 2 H), 1.57–1.39 (m, 8 H), 1.38–1.33 (m, 8 H), 0.98–0.92 (m, 12 H), 0.30 ppm (s, 9 H). ^{13}C{^{1}H} NMR (176 MHz, $CDCl_3$): δ = 156.0, 152.6, 152.5, 148.8, 146.5, 140.8, 140.2, 137.0, 133.4, 129.2, 126.8, 126.72, 126.69, 126.5, 125.9, 125.8, 124.8, 124.6, 124.3, 122.7, 120.1, 115.4, 100.8, 97.7, 70.8, 39.5, 30.6, 29.7, 29.1, 23.9, 23.1, 14.1, 11.2, −0.1 ppm. HRMS (ESI) m/z: $[M]^+$ calcd for $C_{53}H_{61}N_3O_2S_3Si$, 895.3690; found: 895.3730. IR (KBr): $\tilde{\nu}_{max}$ = 2956, 2857, 2149, 1600, 1504, 1484, 1447, 1238, 1035, 855, 798 cm^{-1}. Elemental analysis calcd for $C_{53}H_{61}N_3O_2S_3Si$: C 71.02, H 6.86, N 6.69; found: C 71.10, H 6.84, N 6.70.

Synthesis of 4-(5-((7-(5-ethynyl-thiophen-2-yl)-benzo-[2,1,3]thiadiazol-4-yl)-thiophen-2-yl)-N,N-bis(4-(2-ethyl-hexyl-oxy)phenyl)-aniline (5): A mixture of **4** (0.38 g, 0.42 mmol) and KF (0.12 g, 2.10 mmol) in methylene chloride (6 mL) and methanol (6 mL) was stirred for 30 min at 55 °C. After cooling down the reaction mixture to room temperature, methylene chloride (50 mL) was added and the resulting organic phase washed with water (50 mL) and dried over Na_2SO_4. After solvent removal, the crude product was purified by column chromatography (SiO_2, petroleum ether (40–60 °C)/CH_2Cl_2 = 4/1 v/v) obtaining **5** (0.36 g, 99%) as a purple solid; mp: 88.0 ± 0.5 °C. ^{1}H NMR (700 MHz, $CDCl_3$): δ = 8.14 (d, J = 3.9 Hz, 1 H), 7.97 (d, J = 3.9 Hz, 1 H), 7.87–7.85 (m, 2 H), 7.51 (d, J = 8.7 Hz, 2 H), 7.37 (d, J = 3.8 Hz, 1 H), 7.30 (d, J = 3.8 Hz, 1 H), 7.10 (d, J = 8.7 Hz, 4 H), 6.96 (d, J = 8.5 Hz, 2 H), 6.87 (d, J = 8.7 Hz, 4 H), 3.88–3.81 (m, 4 H), 3.49 (s, 1 H), 1.78–1.71 (m, 2 H), 1.57–1.39 (m, 8 H), 1.38–1.31 (m, 8 H), 0.98–0.90 ppm (m, 12 H). ^{13}C{^{1}H} NMR (176 MHz, $CDCl_3$): δ = 156.0, 152.6, 152.5, 148.8, 146.5, 141.1, 140.2, 136.9, 133.9, 129.2, 126.9, 126.8, 126.72, 126.68, 126.5, 126.10, 125.8, 124.7, 124.5, 122.7, 120.1, 120.0, 115.4, 82.8, 70.8, 39.5, 30.6, 29.1, 23.9, 23.1, 14.1, 11.2 ppm. HRMS (ESI) m/z: $[M]^+$ calcd for $C_{50}H_{53}N_3O_2S_3$, 823.3294; found: 823.3298. IR (KBr): $\tilde{\nu}_{max}$ = 3036, 2956, 2924, 2857, 2137, 2094, 1599, 1503, 1238, 826, 799 cm^{-1}. Elemental analysis calcd for $C_{50}H_{53}N_3O_2S_3$: C 72.87, H 6.48, N 5.51; found: C 72.80, H 6.47, N 5.48.

Synthesis of 5-((5-(7-(5-(4-(bis(4-(2-ethyl-hexyloxy)phenyl)amino)phenyl)thiophen-2-yl)benzo[2,1,3]thiadiazol-4-yl)-thiophen-2-yl)ethynyl)thiophene-2-carbaldehyde (6): A mixture of **5** (0.17 g, 0.21 mmol), 5-bromo-thiophene-2-carbaldehyde (43.9 mg, 0.23 mmol), Pd(PPh$_3$)$_4$ (11.6 mg, 1.0×10^{-2} mmol) and CuI (1.9 mg, 1.0×10^{-2} mmol) in diethylamine (10 mL) was refluxed for 24 h. After cooling down the reaction mixture to room temperature, methylene chloride (50 mL) was added and the resulting organic phase was washed with water (50 mL) and dried over Na_2SO_4. After solvent removal, the crude product was purified by column chromatography (SiO_2, CH_2Cl_2) to yield **6** (0.11 g, 59%) as a violet solid; mp: 95.0 ± 0.5 °C. ^{1}H NMR (700 MHz, $CDCl_3$): δ = 9.90 (s, 1 H), 8.16 (d, J = 3.9 Hz, 1 H), 8.03 (d, J = 3.9 Hz, 1 H), 7.91 (d, J = 7.6 Hz, 1 H), 7.88 (d, J = 7.6 Hz, 1 H), 7. 71 (d, J = 3.9 Hz, 1 H), 7.53–7.50 (m, 2 H), 7.45 (d, J = 3.9 Hz, 1 H), 7.36 (d, J = 3.9 Hz, 1 H), 7.31 (d, J = 3.9 Hz, 1 H), 7.12–7.09 (m, 4 H), 6.97–6.95 (m, 2 H), 6.89–6.86 (m, 4 H), 3.87–3.83 (m, 4 H), 1.77–1.72 (m, 2 H), 1.57–1.39 (m, 8 H), 1.38–1.34 (m, 8 H), 0.98–0.92 ppm (m, 12 H). ^{13}C{^{1}H} NMR (176 MHz, $CDCl_3$): δ = 182.3, 156.1, 152.54, 152.46, 148.9, 146.7, 144.1, 142.6, 140.2, 136.9, 136.0, 134.0, 132.5, 132.4, 129.4, 127.1, 127.0, 126.9, 126.5, 126.2,

125.7, 124.7, 124.2, 122.8, 122.6, 120.0, 115.4, 91.7, 87.5, 70.8, 39.5, 30.6, 29.1, 23.9, 23.1, 14.1, 11.1 ppm. HRMS (ESI) m/z: $[M]^+$ calcd for $C_{55}H_{55}N_3O_3S_4$, 933.3121; found: 933.3105. IR (KBr): $\tilde{\nu}_{max}$ = 3038, 2954, 2924, 2868, 2854, 2180, 1668, 1504, 1238, 827, 798 cm^{-1}. Anal. calcd for $C_{55}H_{55}N_3O_3S_4$: C 70.70, H 5.93, N 4.50; found: C 70.65, H 5.91, N 4.51.

Synthesis of 4-((5-(7-(5-(4-(bis(4-(2-ethyl-hexyloxy)phenyl)amino)phenyl)thiophen-2-yl)benzo[2,1,3]thiadiazol-4-yl)-thiophen-2-yl)ethynyl)benzaldehyde (7): A mixture of **5** (0.17 g, 0.21 mmol), 4-bromo-benzaldehyde (41.9 mg, 0.23 mmol), Pd(PPh$_3$)$_4$ (11.6 mg, 1.0×10^{-2} mmol) and CuI (1.9 mg, 1.0×10^{-2} mmol) in diethylamine (10 mL) was refluxed for 24 h. After cooling down the reaction mixture to room temperature, methylene chloride (50 mL) was added and the resulting organic phase was washed with water (50 mL) and dried over Na_2SO_4. After solvent removal, the crude product was purified by column chromatography (SiO_2, CH_2Cl_2) yielding **7** (0.10 g, 53%) as a violet solid; mp: 97.6 ± 0.5 °C. ^{1}H NMR (700 MHz, $CDCl_3$): δ = 10.05 (s, 1 H), 8.17 (d, J = 3.9 Hz, 1 H), 8.04 (d, J = 3.9 Hz, 1 H), 7.94–7.88 (m, 4 H), 7.71 (d, J = 8.2 Hz, 2 H), 7.52 (d, J = 8.8 Hz, 2 H), 7.45 (d, J = 3.8 Hz, 1 H), 7.31 (d, J = 3.8 Hz, 1 H), 7.11 (d, J = 8.8 Hz, 4 H), 6.97 (d, J = 8.8 Hz, 2 H), 6.87 (d, J = 8.8 Hz, 4 H), 3.88–3.83 (m, 4 H), 1.77–1.71 (m, 2 H), 1.57–1.39 (m, 8 H), 1.38–1.34 (m, 8 H), 0.98–0.92 ppm (m, 12 H). ^{13}C{^{1}H} NMR (176 MHz, $CDCl_3$): δ = 191.3, 156.1, 152.6, 152.5, 148.9, 146.6, 142.0, 140.2, 136.9, 135.5, 133.7, 131.8, 129.6, 129.3, 129.2, 127.02, 126.97, 126.9, 126.5, 126.1, 125.7, 124.7, 124.4, 123.4, 122.7, 120.0, 115.4, 94.1, 87.2, 70.8, 39.5, 30.6, 29.1, 23.9, 23.1, 14.1, 11.1 ppm. HRMS (ESI) m/z: $[M]^+$ calcd for $C_{57}H_{57}N_3O_3S_3$, 927.3557; found: 927.3620. IR (KBr): $\tilde{\nu}_{max}$ = 3036, 2955, 2924, 2857, 2193, 1701, 1482, 1500, 1235, 827, 798 cm^{-1}. Elemental analysis calcd for $C_{57}H_{57}N_3O_3S_3$: N 4.53, C 73.75, H 6.19; found: N 4.52, C 73.72, H 6.17.

Synthesis of 2-cyano-3-(5-((5-(7-(5-(4-(bis(4-(2-ethyl-hexyloxy)-phenyl)amino)phenyl)-thiophen-2-yl)benzo[2,1,3]thiadiazol-4-yl)-thiophen-2-yl)ethynyl)-thiophen-2-yl)acrylic acid (G1): A mixture of **6** (0.10 g, 0.11 mmol), cyano-acetic acid (45.9 mg, 0.54 mmol) and ammonium acetate (2.8 mg, 3.6×10^{-2} mmol) in acetic acid (10 mL) was refluxed overnight. After cooling down the reaction to room temperature, the mixture was poured into water (200 mL) to obtain a precipitate that was collected by filtration and washed with water. The crude product was purified by column chromatography (SiO_2, CH_2Cl_2/MeOH = 10/1 v/v) to afford **G1** (43.1 mg, 40%) as a violet solid. ^{1}H NMR (700 MHz, CD_2Cl_2/CF_3COOD): δ = 8.58–8.40 (br, 4 H), 8.36–7.89 (br, 7 H), 7.55–7.04 (br, 10 H), 3.89–3.82 (br, 4 H), 1.76–1.70 (br, 2 H), 1.60–1.32 (br, 16 H), 1.03–0.90 ppm (br, 12 H). HRMS (ESI) m/z: $[M−H]^-$ calcd for $C_{58}H_{55}N_4O_4S_4$, 999.3101; found: 999.3917. IR (KBr): $\tilde{\nu}_{max}$ = 3432, 2960, 2920, 2876, 2850, 2214, 2173, 1617, 1505, 1378, 1237, 825, 798 cm^{-1}. Elemental analysis for $C_{58}H_{56}N_4O_4S_4$: C 69.57, H 5.64, N 5.60; found: C 69.45, H 5.66, N 5.59.

Synthesis of 2-cyano-3-(4-((5-(7-(5-(4-(bis(4-(2-ethyl-hexyloxy)-phenyl)amino)phenyl)-thiophen-2-yl)benzo[2,1,3]thiadiazol-4-yl)-thiophen-2-yl)ethynyl)-phenyl)acrylic acid (G2): A mixture of **7** (86.4 mg, 9.3×10^{-2} mmol), cyano-acetic acid (39.6 mg, 0.47 mmol) and ammonium acetate (2.4 mg, 3.1×10^{-2} mmol) in acetic acid (10 mL) was refluxed overnight. After cooling down the reaction to room temperature, the mixture was poured into water (200 mL) to obtain a precipitate that was collected by filtration and washed with water. The crude product was purified by column chromatography (SiO_2, CH_2Cl_2/MeOH = 10:1 v/v) to give **G2** (35.4 mg, 38%) as a violet solid. ^{1}H NMR (700 MHz, CD_2Cl_2/CF_3COOD): δ = 8.59–8.41 (br, 4 H), 8.35–7.90 (br, 9 H), 7.55–7.05 (br, 10 H), 3.88–3.83 (br, 4 H), 1.77–1.71 (br, 2 H), 1.60–1.32 (br, 16 H), 1.03–0.90 ppm (br, 12 H). HRMS (ESI) m/z: $[M−H]^-$ calcd for $C_{60}H_{57}N_4O_4S_3$, 993.3536; found: 993.4329. IR (KBr): $\tilde{\nu}_{max}$ = 3432, 2956, 2925, 2870, 2855, 2216, 2193,

These are not the final page numbers! ↗↗

[1] a) Y. Ooyama, Y. Harima, *ChemPhysChem* **2012**, *13*, 4032; b) A. Mishra, M. K. R. Fischer, P. Bäuerle, *Angew. Chem. Int. Ed.* **2009**, *48*, 2474; *Angew. Chem.* **2009**, *121*, 2510.

[2] a) S. Zhang, X. Yang, Y. Numata, L. Han, *Energy Environ. Sci.* **2013**, *6*, 1443; b) A. Hagfeldt, G. Boschloo, L. Sun, L. Kloo, H. Pettersson, *Chem. Rev.* **2010**, *110*, 6595; c) L. Wang, X. Fang, Z. Zhang, *Renewable Sustainable Energy Rev.* **2010**, *14*, 3178.

[3] a) M. K. Nazeeruddin, E. Baranoff, M. Grätzel, *Sol. Energy* **2011**, *85*, 1172; b) N. Robertson, *Angew. Chem. Int. Ed.* **2006**, *45*, 2338; *Angew. Chem.* **2006**, *118*, 2398.

[4] a) A. Listorti, B. O'Regan, J. R. Durrant, *Chem. Mater.* **2011**, *23*, 3381; b) Z. Ning, H. Tian, *Chem. Commun.* **2009**, 5483; c) S. Kim, J. K. Lee, S. O. Kang, J. Ko, J. H. Yum, S. Fantacci, F. De Angelis, D. Di Censo, M. K. Nazeeruddin, M. Grätzel, *J. Am. Chem. Soc.* **2006**, *128*, 16701.

[5] T. Marinado, K. Nonomura, J. Nissfolk, M. K. Karlsson, D. P. Hagberg, L. Sun, S. Mori, A. Hagfeldt, *Langmuir* **2010**, *26*, 15476.

[6] a) R. Katoh, A. Furube, S. Mori, M. Miyashita, K. Sunahara, N. Koumura, K. Hara, *Energy Environ. Sci.* **2009**, *2*, 542; b) K. Hara, Z.-S. Wang, T. Sato, A. Furube, R. Katoh, H. Sugihara, Y. Dan-oh, C. Kasada, A. Shimpo, S. Suga, *J. Phys. Chem. B* **2005**, *109*, 15476.

[7] As recent examples: a) S. Zhang, A. Islam, X. Yang, C. Qin, K. Zhang, Y. Numata, H. Chen, L. Han, *J. Mater. Chem. A* **2013**, *1*, 4812; b) L. Han, A. Islam, H. Chen, C. Malapaka, B. Chiranjeevi, S. Zhang, X. Yang, M. Yanagida, *Energy Environ. Sci.* **2012**, *5*, 6057; c) C.-M. Lan, H.-P. Wu, T.-Y. Pan, C.-W. Chang, W.-S. Chao, C.-T. Chen, C.-L. Wang, C.-Y. Lin, E. W.-G. Diau, *Energy Environ. Sci.* **2012**, *5*, 6460.

[8] Y. Wu, W. Zhu, *Chem. Soc. Rev.* **2013**, *42*, 2039.

[9] J. Y. Li, A. Ziegler, G. Wegner, *Chem. Eur. J.* **2005**, *11*, 4450.

[10] Y.-S. Yen, C.-T. Lee, C.-Y. Hsu, H.-H. Chou, Y.-C. Chen, J. T. Lin, *Chem. Asian J.* **2013**, *8*, 809.

[11] a) W. Ying, J. Yang, M. Wielopolski, T. Moehl, J.-E. Moser, P. Comte, J. Hua, S. M. Zakeeruddin, H. Tian, M. Grätzel, *Chem. Sci.* **2014**, *5*, 206; b) K. Pei, Y. Wu, A. Islam, Q. Zhang, L. Han, H. Tian, W. Zhu, *ACS Appl. Mater. Interfaces* **2013**, *5*, 4986; c) K. Pei, Y. Wu, W. Wu, Q. Zhang, B. Chen, H. Tian, W. Zhu, *Chem. Eur. J.* **2012**, *18*, 8190.

[12] W. Li, Y. Wu, Q. Zhang, H. Tian, W. Zhu, *ACS Appl. Mater. Interfaces* **2012**, *4*, 1822.

[13] F. Zhang, K.-J. Jiang, J.-H. Huang, C.-C. Yu, S.-G. Li, M.-G. Chen, L.-M. Yang, Y.-L. Song, *J. Mater. Chem. A* **2013**, *1*, 4858.

[14] a) M. Zhang, Y. Wang, M. Xu, W. Ma, R. Li, P. Wang, *Energy Environ. Sci.* **2013**, *6*, 2944; b) Y. Wu, M. Marszalek, S. M. Zakeeruddin, Q. Zhang, H. Tian, M. Grätzel, W. Zhu, *Energy Environ. Sci.* **2012**, *5*, 8261; c) Y. Wu, X. Zhang, W. Li, Z.-S. Wang, H. Tian, W. Zhu, *Adv. Energy Mater.* **2012**, *2*, 149; d) H.-H. Chou, Y.-C. Chen, H.-J. Huang, T.-H. Lee, J. T. Lin, C. Tsai, K. Chen, *J. Mater. Chem.* **2012**, *22*, 10929; e) S. Haid, M. Marszalek, A. Mishra, M. Wielopolski, J. Teuscher, J.-E. Moser, R. Humphry-Baker, S. M. Zakeeruddin, M. Grätzel, P. Bäuerle, *Adv. Funct. Mater.* **2012**, *22*, 1291; f) W. Zhu, Y. Wu, S. Wang, W. Li, X. Li, J. Chen, Z.-S. Wang, H. Tian, *Adv. Funct. Mater.* **2011**, *21*, 756; g) D. H. Lee, M. J. Lee, H. M. Song, B. J. Song, K. D. Seo, M. Pastore, C. Anselmi, S. Fantacci, F. De Angelis, M. K. Nazeeruddin, M. Grätzel, H. K. Kim, *Dyes Pigm.* **2011**, *91*, 192; h) J.-J. Kim, H. Choi, J.-W. Lee, M.-S. Kang, K. Song, S. O. Kang, J. Ko, *J. Mater. Chem.* **2008**, *18*, 5223; i) M. Velusamy, K. R. J. Thomas, J. T. Lin, Y.-C. Hsu, K.-C. Ho, *Org. Lett.* **2005**, *7*, 1899; j) X. Wang, J. Yang, H. Yu, F. Li, L. Fan, W. Sun, Y. Liu, Z. Y. Koh, J. Pan, W.-L. Yim, L. Yan, Q. Wang, *Chem. Commun.* **2014**, *50*, 3965.

[15] a) C. Teng, X. C. Yang, C. Yang, H. Tian, S. F. Li, X. Wang, A. Hagfeldt, L. Sun, *J. Phys. Chem. C* **2010**, *114*, 11305; b) J. Song, F. Zhang, C. Li, W. Liu, B. Li, Y. Huang, Z. Bo, *J. Phys. Chem. C* **2009**, *113*, 13391.

[16] H. Tian, X. Yang, R. Chen, R. Zhang, A. Hagfeldt, L. Sun, *J. Phys. Chem. C* **2008**, *112*, 11023.

[17] R. Grisorio, G. Allegretta, P. Mastrorilli, G. P. Suranna, *Macromolecules* **2011**, *44*, 7977.

[18] A. A. Gorman, M. A. Rodgers, *Chem. Soc. Rev.* **1981**, *10*, 205.

[19] H. D. Roth, *Acc. Chem. Res.* **1984**, *17*, 180.

[20] R. Grisorio, G. Allegretta, G. P. Suranna, P. Mastrorilli, A. Loiudice, A. Rizzo, M. Mazzeo, G. Gigli, *J. Mater. Chem.* **2012**, *22*, 19752.

[21] J.-L. Bredas, *Mater. Horiz.* **2014**, *1*, 17.

[22] a) K. Hara, Y. Dan-oh, C. Kasada, Y. Ohga, A. Shinpo, S. Suga, K. Sayama, H. Arakawa, *Langmuir* **2004**, *20*, 4205; b) Z.-S. Wang, Y. Cui, Y. Dan-oh, C. Kasada, A. Shinpo, K. Hara, *J. Phys. Chem. C* **2008**, *112*, 17011.

[23] J. Bisquert, *J. Electroanal. Chem.* **2010**, *646*, 43.

[24] J. Bisquert, F. Fabregat-Santiago, I. Mora-Sero', G. Garcia-Belmonte, S. Gimnez, *J. Phys. Chem.* **2009**, *113*, 17278.

[25] S. R. Raga, E. M. Barea, F. Fabregat-Santiago, *J. Phys. Chem. Lett.* **2012**, *3*, 1629.

[26] a) E. M. Barea, V. Gonzalez-Pedro, T. Ripolles-Sanchis, H.-P. Wu, L.-L. Li, C.-Y. Yeh, E. W.-G. Diau, J. Bisquert, *J. Phys. Chem. C* **2011**, *115*, 10898; b) E. M. Barea, J. Ortiz, F. J. Paya, F. Fernandez-Lazaro, F. Fabregat-Santiago, A. Sastre-Santos, J. Bisquert, *Energy Environ. Sci.* **2010**, *3*, 1985.

[27] a) M. Pastore, E. Mosconi, F. De Angelis, *J. Phys. Chem. C* **2012**, *116*, 5965; b) X. Li, A. Reynal, P. Barnes, R. Humphry-Baker, S. M. Zakeeruddin, F. De Angelis, B. C. O'Regan, *Phys. Chem. Chem. Phys.* **2012**, *14*, 15421; c) X. Jiang, K. M. Karlsson, E. Gabrielsson, E. M. J. Johansson, M. Quintana, M. Karlsson, L. Sun, G. Boschloo, A. Hagfeldt, *Adv. Funct. Mater.* **2011**, *21*, 2944.

[28] C. M. Cardona, W. Li, A. E. Kaifer, D. Stockdale, G. C. Bazan, *Adv. Mater.* **2011**, *23*, 2367.

[29] Gaussian 09, revision D.01, M. J. Frisch, G. W. Trucks, H. B. Schlegel, G. E. Scuseria, M. A. Robb, J. R. Cheeseman, G. Scalmani, V. Barone, B. Mennucci, G. A. Petersson, H. Nakatsuji, M. Caricato, X. Li, H. P. Hratchian, A. F. Izmaylov, J. Bloino, G. Zheng, J. L. Sonnenberg, M. Hada, M. Ehara, K. Toyota, R. Fukuda, J. Hasegawa, M. Ishida, T. Nakajima, Y. Honda, O. Kitao, H. Nakai, T. Vreven, J. A. Montgomery, Jr., J. E. Peralta, F. Ogliaro, M. Bearpark, J. J. Heyd, E. Brothers, K. N. Kudin, V. N. Staroverov, R. Kobayashi, J. Normand, K. Raghavachari, A. Rendell, J. C. Burant, S. S. Iyengar, J. Tomasi, M. Cossi, N. Rega, J. M. Millam, M. Klene, J. E. Knox, J. B. Cross, V. Bakken, C. Adamo, J. Jaramillo, R. Gomperts, R. E. Stratmann, O. Yazyev, A. J. Austin, R. Cammi, C. Pomelli, J. W. Ochterski, R. L. Martin, K. Morokuma, V. G. Zakrzewski, G. A. Voth, P. Salvador, J. J. Dannenberg, S. Dapprich, A. D. Daniels, O. Farkas, J. B. Foresman, J. V. Ortiz, J. Cioslowski, D. J. Fox, Gaussian, Inc., Wallingford CT, **2009**.
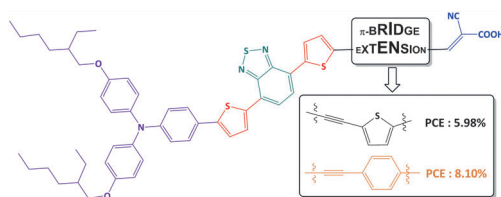
FULL PAPERS

R. Grisorio, L. De Marco,* R. Agosta,
R. Iacobellis, R. Giannuzzi, M. Manca,
P. Mastrorilli, G. Gigli, G. P. Suranna*

■■ – ■■

Enhancing Dye-Sensitized Solar Cell Performances by Molecular Engineering: Highly Efficient π-Extended Organic Sensitizers

Can I have an extension please? Two new π-extended D–A–π–A dyes are synthesized for application in dye-sensitized solar cells (DSSCs). The introduction of an ethynylene–phenylene moiety in the π-bridge leads to remarkably higher efficiency in DSSCs compared to the sensitizer with the ethynylene–thienylene spacer due to higher electron injection, inhibition of back electron-transfer as well as dark current.

These are not the final page numbers! ↗↗